Oxygen storage capacity measurements of three-way catalysts under transient conditions

C. Descorme, Rachida Taha, Najat Mouaddib-Moral, Daniel Duprez

Oxygen storage capacity measurements of three-way catalysts under transient conditions

Claude Descorme [a,*], Rachid Taha [a], Najat Mouaddib-Moral [b], Daniel Duprez [a]

[a] *Laboratoire de Catalyse en Chimie Organique (LACCO) — UMR CNRS 6503, Université de Poitiers, 40 avenue du Recteur Pineau, F-86022 Poitiers Cedex, France*

[b] *Renault Automobiles, Centre Technique de Lardy, 1 Allée de Cornuel, 91510 Lardy, France*

Oxygen storage capacity (OSC) measurements at 450°C were carried out on 10 different alumina and ceria-alumina supported Pd, Pt, Rh, PdRh and PtRh catalysts. Experiments were performed under both transient (0.5 and 1 Hz) and stationary reaction conditions using a mass spectrometer for the gas phase analysis every 100 ms. OSC was shown to be strongly dependent on the metal nature — oxidized or reduced. Rh appeared to be the best OSC promoter. Furthermore, ceria addition to the alumina support strongly enhances the OSC. In fact looking at the OSC values, a factor of 3 was evidenced between Pt/Al_2O_3 and Rh/Al_2O_3 and an additional factor of about 12 between Rh/Al_2O_3 and Rh/CeO_2-Al_2O_3. The metal oxides relative stability as well as the metal electronic configuration were shown to be strongly influent on the overall reactivity of the catalyst. Additional kinetic studies showed that the oxide reduction rate under CO is slower than the oxide oxidation rate under O_2. Finally a general scheme for the oxygen storage process is proposed and discussed.

Keywords: Oxygen storage; Transient conditions; Stationary conditions; Palladium; Platinum; Rhodium; Catalyst; Alumina; Ceria-alumina

1. Introduction

In the field of three-way catalysis (TWC), oxygen storage is a crucial point. As a result, lots of studies have been devoted to oxygen storage capacity (OSC) measurements [1–9]. The performances of automotive pollution control catalysts have been shown to somehow correlates with the OSC of these solids. In fact, the OSC measurement has been considered as a potential indication of the catalyst state — active or inactive — for on-board diagnostic (OBD) applications [10–14]. However, up to now, OSC measurements have been carried out under ideal conditions, in a continuous mode [1,7]. Such measurement conditions are far from real post-combustion operating conditions, when the exhaust gas composition rapidly oscillates between hydrocarbon-rich and hydrocarbon-poor mixtures.

This paper deals with the development of a new OSC measurement technique. OSC could be measured in a transient regime by injection of alternate CO or O_2 pulses every 1 or 2 s ($F = 1$ or 0.5 Hz). Such measurements conditions were shown to be appropriate to simulate the fluctuations in the real exhaust gas composition.

This technique was applied to the study of two series of Pt-, Rh- and Pd-based model three-way catalysts. Our study will concentrate on both the effect of ceria on the OSC and the influence of the nature of the noble metal on the CO oxidation catalytic reaction.

* Corresponding author. Tel.: +33-5-49-45-39-97; fax: +33-5-49-45-34-99.
E-mail address: claude.descorme@univ-poitiers.fr (C. Descorme).

2. Experimental

2.1. Catalysts preparation

Alumina support (A) was obtained from γ-alumina ($100\,m^2\,g^{-1}$) directly supplied by Institut Français du Pétrole (IFP, France). After treatment at 900°C, the δ-Al_2O_3 phase is predominant.

A 12% CeO_2-Al_2O_3 support (CA) was prepared by impregnation of the alumina support with an aqueous solution of an ammonium and cerium nitrate ($Ce(NH_4)_2(NO_3)_6$). After evaporation and drying, the CeO_2-Al_2O_3 support is calcined at 450°C for 5 h.

Monometallic catalysts were prepared by incipient wetness impregnation of the support either with an aqueous solution of diaminodinitro platinum(II) ($Pt(NH_3)_2(NO_2)_2$) or with a solution of palladium(II) diacetylacetonate ($Pd(C_5H_7O_2)_2$) in acetone. Bimetallic catalysts were subsequently prepared by impregnation of the pre-reduced monometallic catalyst with an aqueous solution of Rh^{3+} ($Rh(NO_3)_3$). Every metal precursor was chlorine-free. In fact, chlorine was found to decrease both oxygen mobility at the oxides surface and the OSC [15–18]. Such an effect of chlorine could result in an inhibition of the oxygen storage.

After impregnation Pt-based (series 1) and Pd-based (series 2) catalysts were dried and further calcined at 350°C [19]. Every catalyst was further aged under 10% H_2O + 1% O_2 at 900°C for 2 h [20]. In fact, fresh catalysts were too active so that oxygen storage kinetics could not be accessed.

The composition of the catalysts is, respectively, given in Tables 1 and 2 for series 1 and 2 samples.

Table 1
Metal loading for the different bimetallic PtRh-based alumina (A) and ceria-alumina (CA) supported catalysts (series 1)

Catalyst	wt.%		μmol of metal atoms per gram of catalyst
	Pt	Rh	
PtA	1.17	0.00	60
PtCA	1.00	0.00	51.3
PtRhA[a]	0.70	0.21	55.3
PtRhCA[a]	0.60	0.21	51.2
RhA	0.00	0.50	49.5
RhCA	0.00	0.53	51.4

[a] The metallic phase consist in 35% Rh and 65% Pt or Pd.

Table 2
Metal loading for the different bimetallic PdRh-based alumina (A) and ceria-alumina (CA) supported catalysts (series 2)

Catalyst	wt.%		μmol of metal atoms per gram of catalyst
	Pd	Rh	
PdA	0.50	0.00	47
PdCA	0.50	0.00	47
PdRhA[a]	0.33	0.17	47
PdRhCA[a]	0.33	0.17	47
RhA	0.00	0.50	49.5
RhCA	0.00	0.53	51.4

[a] The metallic phase consist in 35% Rh and 65% Pt or Pd.

The composition of the metallic phase was adjusted so that every catalyst contains about 50 μmol of metal atoms per gram of catalyst.

2.2. Experimental setup

The apparatus used for this set of experiments is dedicated to the study of reactions — $CO + O_2$ in our case — carried out under transient conditions at any given frequency lower than 1 Hz. This system consists in two parts: the gas manifold and the mass spectrometer.

Reactants (CO and O_2) flows are regulated using mass flow controllers. Before the reactor entrance, reactants are mixed with a 1% Ar in He carrier gas ($100\,cm^3\,min^{-1}$). Any kind of CO/(1% Ar + He) and O_2/(1% Ar + He) mixtures could be obtained. For this study, 2% CO and 1% O_2 mixtures were used. Reactant injections were controlled using automated injection valves. Alternate CO and O_2 injections may take place at a frequency as high as 1 Hz. To optimize the response time, the dead volume was reduce to less than $2.5\,cm^3$, including the whole reaction circuit from the automated valve up to the capillary tube before the mass spectrometer.

A 2 mg sample, diluted in 18 mg cordierite, is placed in a straight Pyrex reactor and pretreated under pure helium at 450°C (ramp rate: $2°C\,min^{-1}$) for 15 min. Reactions are carried out at 450°C. Despite of the low sample weight, reproducibility was checked to be better than 5%.

The experiment consists in five different steps, as presented in Fig. 1 — (i) OSC measurement at 450°C under transient conditions: alternate 2% CO

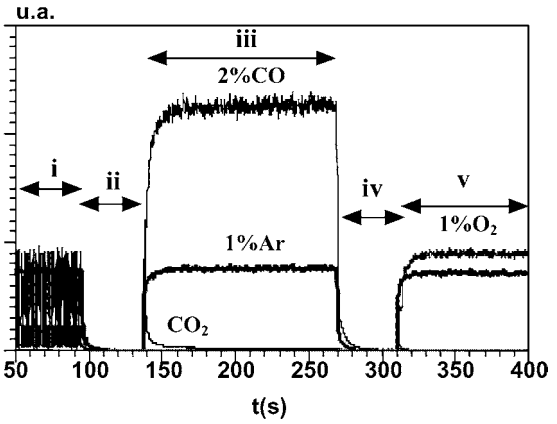

Fig. 1. One typical experiment. General scheme for the measurement progression.

or 1% O_2 pulses at a frequency of 1 or 0.5 Hz for 10 min. Carrier gas is 1% Ar in He. The last pulse is O_2: (ii) outgassing under pure He for 30 s; (iii) step change from 0 to 2% CO (2 min) at 450°C. Carrier gas is 1% Ar in He. The Ar signal is used as a reference to deduced the dead volume of the reactor and to recalculate the inlet CO step change from 0 to 2%: (iv) outgassing under pure He for 30 s; (v) step change from 0 to 1% O_2 (2 min) at 450°C. Carrier gas is again 1% Ar in He. The Ar signal is used as a reference.

The evolution of the gas phase composition is followed by mass spectrometry. Masses $m/e = 4$ (He), 28 (CO), 32 (O_2), 44 (CO_2) and 40 (Ar) are monitored every 0.1 s. The global experimental setup used for both OSC measurements is schematized in Fig. 2.

All the results presented below will be expressed per gram of solid. Every sample consisted of 2 mg catalyst plus 18 mg cordierite for a total of 20 mg of solid.

3. Results and discussion

3.1. CO and O_2 steps — stationary regime

Data deduced from the second part of the OSC measurement being necessary for the interpretation of the results obtained in the first part, the results drawn from the second part of the experiment will be described first for a better readability of our manuscript.

In that second part of the experiment, OSC measurements are carried out at 450°C under "stationary" conditions. All samples are subsequently submitted to a 2 min long 2% CO step (step (iii), see Fig. 1) and a 2 min long 1% O_2 step (step (v), see Fig. 1) with intermediate outgassing under pure He for 10 min. Evolutions of the unconverted CO and the produced CO_2 during step (iii) (see Fig. 1) and the unconverted O_2 during step (v) (see Fig. 1) are monitored as a function of time. Examples are given in Figs. 3 and 4 for Pd-based (series 2) and Pt-based (series 1) catalysts, respectively. The amounts of CO and O_2 or CO_2, respectively, consumed or produced were expressed as differential amounts of molecules consumed or produced per gram of solid and per unit time ($\mu mol\, g^{-1}\, \Delta t^{-1}$). Differential calculations were performed using 0.1 s time increments. Every points on the curves correspond to the amount of CO, CO_2 or O_2 consumed or produced during the last 0.1 s. Cumulated amounts of CO and O_2 consumption and CO_2 production could be derived from the integration of these CO, CO_2 and O_2 curves. An example is given in Fig. 5 for Pt-based catalysts (series 1).

Table 3 summarizes the amounts of CO consumed and CO_2 produced during CO step and the amounts of O_2 consumed during O_2 step at time t equals 0.5, 1, 5 and 40 s for all 10 catalysts under study. A close look to this table shows that alumina-supported catalysts have a very low OSC. On the opposite, ceria-containing catalysts have the highest activity towards oxygen storage. These catalysts may be classified in descending order as follows: Rh/CeO_2-Al_2O_3 (RhCA) > $PtRh/CeO_2$-Al_2O_3 (PtRhCA) > $PdRh/CeO_2$-Al_2O_3 (PdRhCA) > Pd/CeO_2-Al_2O_3 (PdCA) > Pt/CeO_2-Al_2O_3 (PtCA) > Rh/Al_2O_3 (RhA) $\cong$ $PtRh/Al_2O_3$ (PtRhA) > $PdRh/Al_2O_3$ (PdRhA) > Pt/Al_2O_3 (PtA) $\cong$ Pd/Al_2O_3 (PdA). Differences in OSC among these "aged" catalysts could be explained by the different sintering modes for Rh, Pt and Pd [21–23]. Furthermore, this reactivity ordering may be explained by the presence of both Rh and ceria. Rhodium strongly enhance the reducibility of ceria so that the OSC is greatly improved.

Furthermore, one can see that $PtRh/CeO_2$-Al_2O_3 (PtRhCA) behaves like a pure rhodium catalyst. This would indicate that (i) either Pt and Rh particles are distinct and Rh particles are in direct

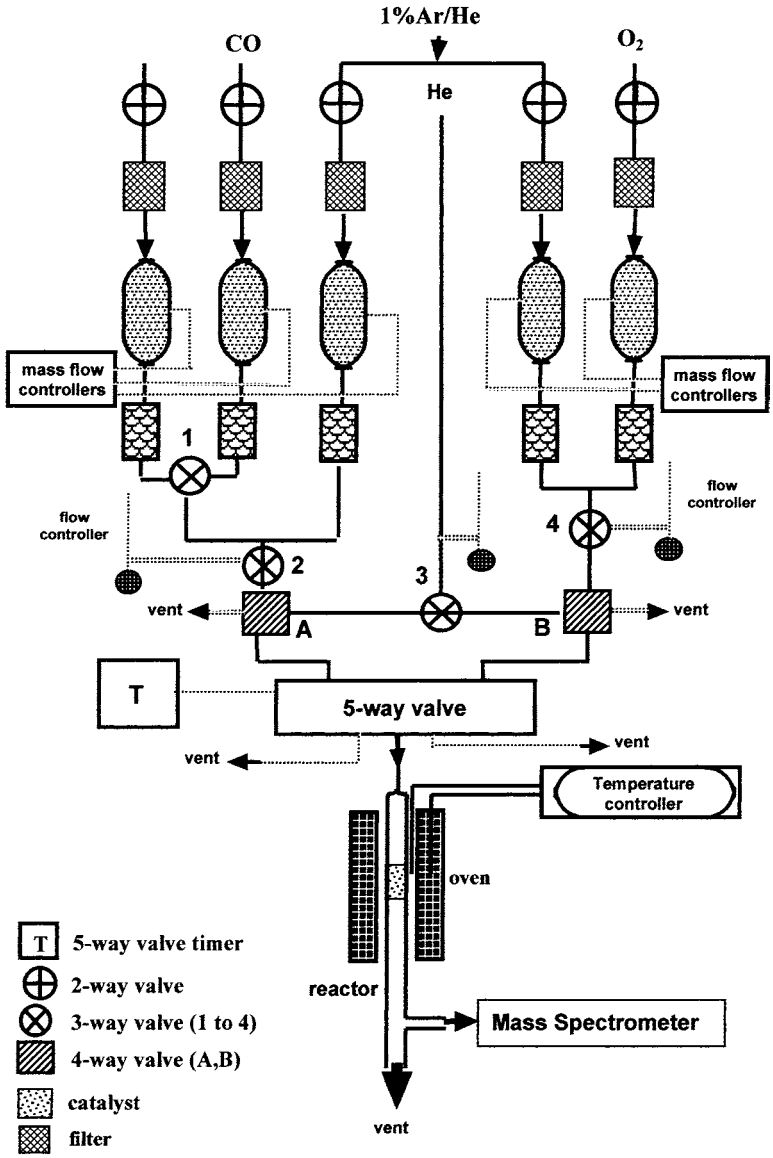

Fig. 2. Flow-sheet of the homemade apparatus used for OSC measurements.

interaction with ceria or (ii) Rh segregates at the surface of PtRh bimetallic particles. On the opposite, PdRh/CeO_2-Al_2O_3 (PdRhCA) reacts as pure Pd and we concluded that (i) either Pd and Rh particles are distinct and Rh particles do not interact with ceria or (ii) Pd segregates at the surface of PdRh bimetallic particles. In one case almost pure rhodium is the active surface and OSC is high, in the second case almost pure palladium is the active surface and OSC is low.

Finally, initial rates for CO consumption and CO_2 formation upon CO step and for O_2 consumption upon O_2 step are reported in Fig. 6 for both alumina (A) and ceria-alumina (CA) supported catalysts. Initial rates

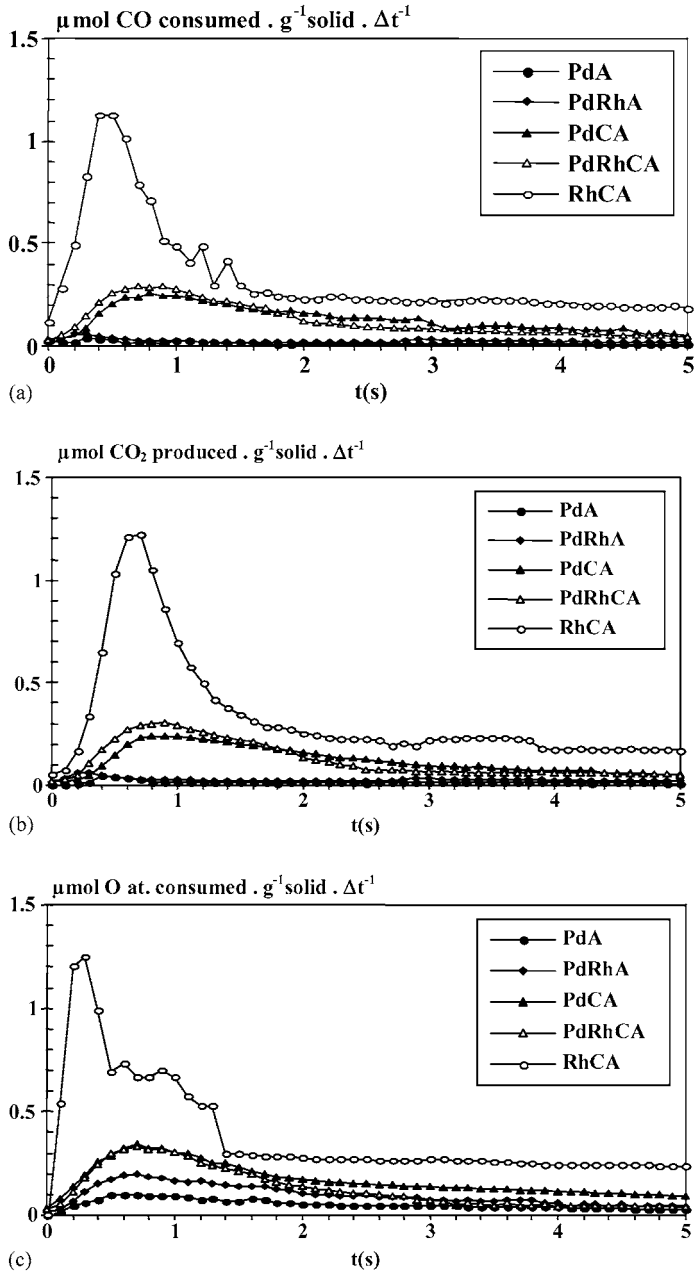

Fig. 3. CO and O_2 step changes on pre-oxidized on bimetallic PdRh-based alumina (A) and ceria-alumina (CA) supported catalysts at 450°C: (a) differential CO consumption during CO step; (b) differential CO_2 formation during CO step; (c) differential O_2 consumption during O_2 step expressed in $\mu\text{mol}\,\text{g}^{-1}\,\Delta t^{-1}$ ($\Delta t = 0.1$ s).

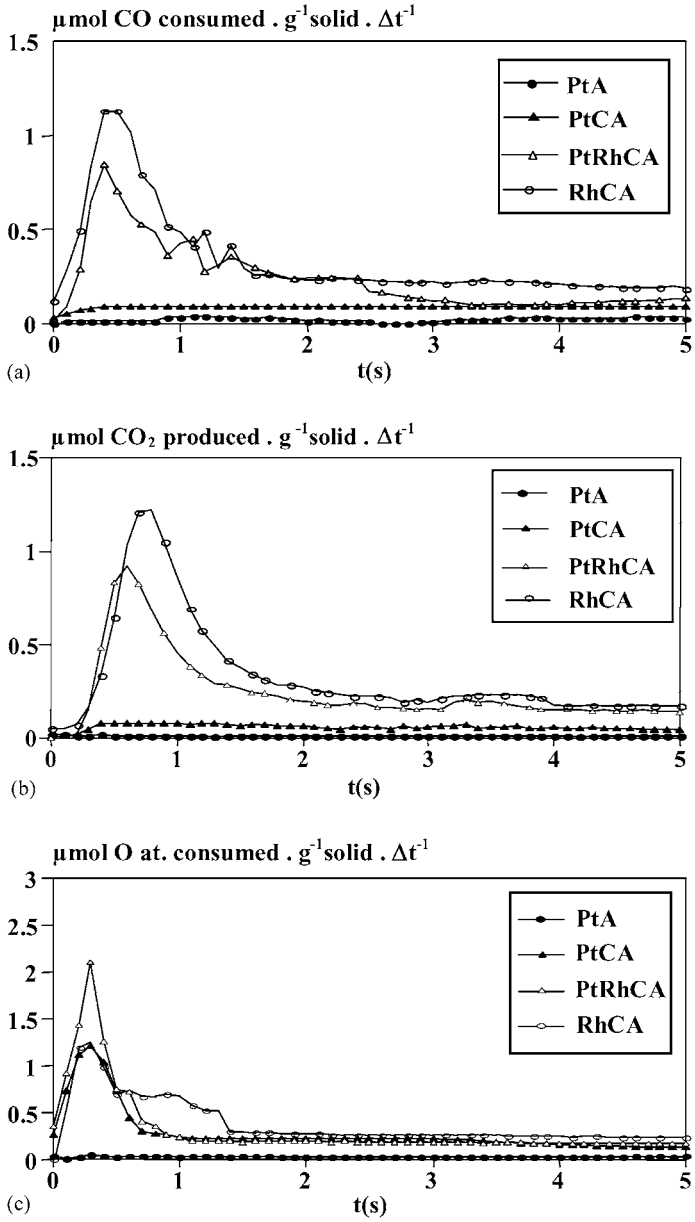

Fig. 4. CO and O_2 step changes on pre-oxidized on bimetallic PtRh-based alumina (A) and ceria-alumina (CA) supported catalysts at 450°C: (a) differential CO consumption during CO step; (b) differential CO_2 formation during CO step; (c) differential O_2 consumption during O_2 step expressed in $\mu\text{mol}\,g^{-1}\,\Delta t^{-1}$ ($\Delta t = 0.1$ s).

were deduced from the slopes, extrapolated at zero time, of the plots presented in Fig. 5. One may immediately conclude that reoxidation of the catalysts by molecular oxygen is much faster than the reduction under CO.

3.2. High frequency alternate CO and O_2 pulses — transient regime

As stated in Section 2, every experiment starts with the OSC measurement at 450°C under transient

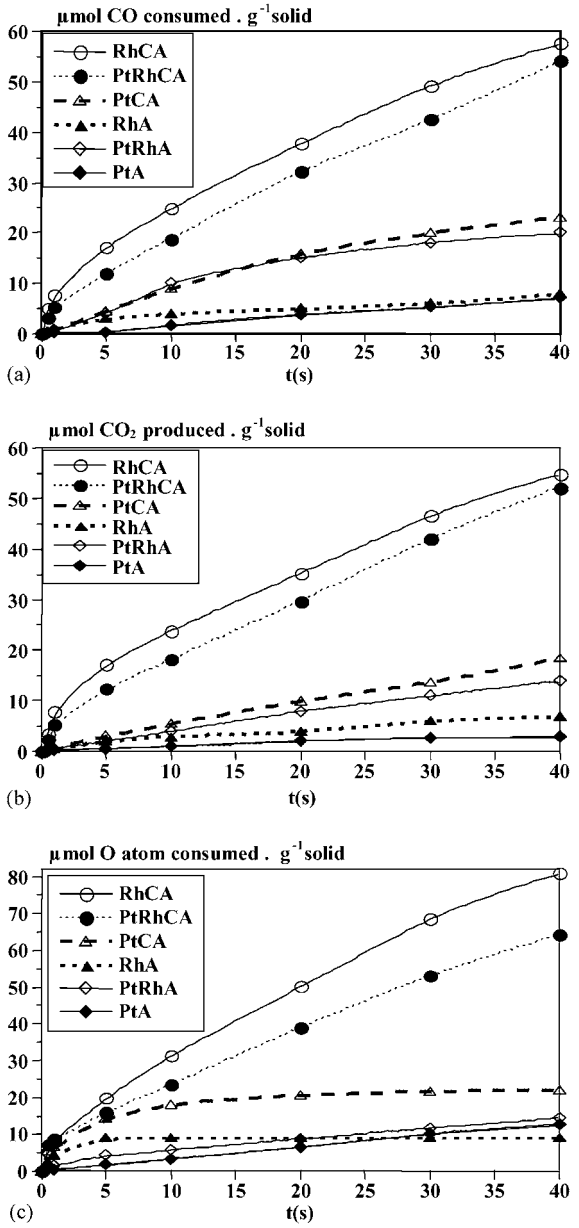

Fig. 5. Cumulative curves for CO consumption and CO_2 formation during CO step and for O_2 consumption during O_2 step on bimetallic PtRh-based alumina (A) and ceria-alumina (CA) supported catalysts at 450°C. Curves were built from points acquired every 0.1 s. For sake of clarity, only a few experimental points are displayed.

Table 3
CO and O_2 steps[a]

	$Q_{0.5}$	Q_1	Q_5	Q_{40}
PdA				
CO[b]	0.2	0.3	0.7	3.9
CO_2[b]	0.2	0.3	0.7	3.2
O_2[c]	0.4	0.9	2.7	4.4
PtA				
CO[b]	0.1	0.3	0.3	7
CO_2[b]	0.1	0.2	0.6	3
O_2[c]	0.2	0.4	1.7	13
RhA				
CO[b]	0.4	0.9	3.0	8
CO_2[b]	0.3	0.6	2.0	7
O_2[c]	2.4	4.2	9.1	9
PdRhA				
CO[b]	0.2	0.4	1.1	6.6
CO_2[b]	0.2	0.4	1.3	6.1
O_2[c]	0.4	1.3	4.8	6.5
PtRhA				
CO[b]	0.4	0.7	4.0	20
CO_2[b]	0.3	0.6	2.0	14
O_2[c]	0.8	1.5	4.2	14
PdCA				
CO[b]	0.8	2.0	6.7	15.3
CO_2[b]	0.8	1.7	6.2	15.2
O_2[c]	1.3	2.9	8.7	20.1
PtCA				
CO[b]	0.5	0.8	4.5	23
CO_2[b]	0.3	0.7	3.1	19
O_2[c]	5.3	6.6	14.3	22
RhCA				
CO[b]	4.9	7.8	17.2	58
CO_2[b]	3.5	7.9	17.2	55
O_2[c]	5.4	8.7	19.7	81
PdRhCA				
CO[b]	1.3	2.7	6.4	11.9
CO_2[b]	1.1	2.6	6.2	11.9
O_2[c]	1.2	2.8	6.5	13.4
PtRhCA				
CO[b]	3.1	5.4	12.0	54
CO_2[b]	2.4	5.2	12.3	52
O_2[c]	7.2	8.6	15.9	64

[a] Cumulative amounts "Q_t" (µmol g^{-1}) consumed or produced between zero time and time t (s) on Pt, Pd, Rh, PtRh- and PdRh-based alumina (A) and ceria-alumina (CA) supported catalysts.

[b] CO consumed or CO_2 formed (µmol g^{-1}) after the CO step.

[c] O_2 consumed (µmol O atoms g^{-1}) after the O_2 step.

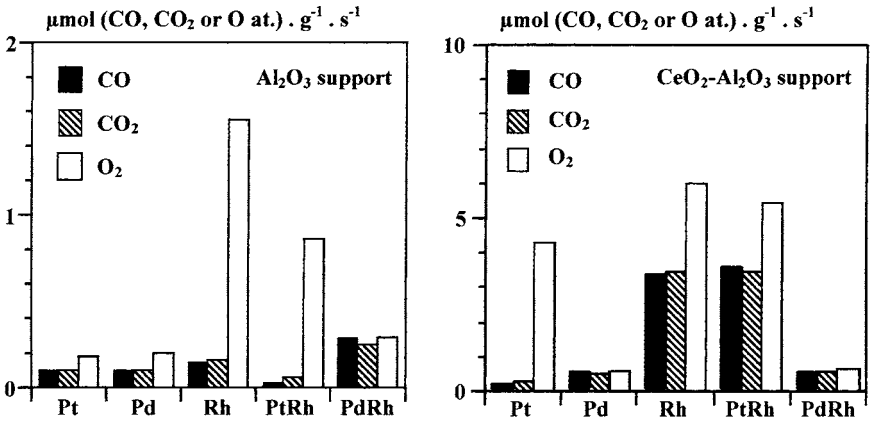

Fig. 6. Comparison of the initial rates for CO consumption and CO_2 formation during CO step and for O_2 consumption during O_2 step on alumina (A) and ceria-alumina (CA) supported catalysts at 450°C.

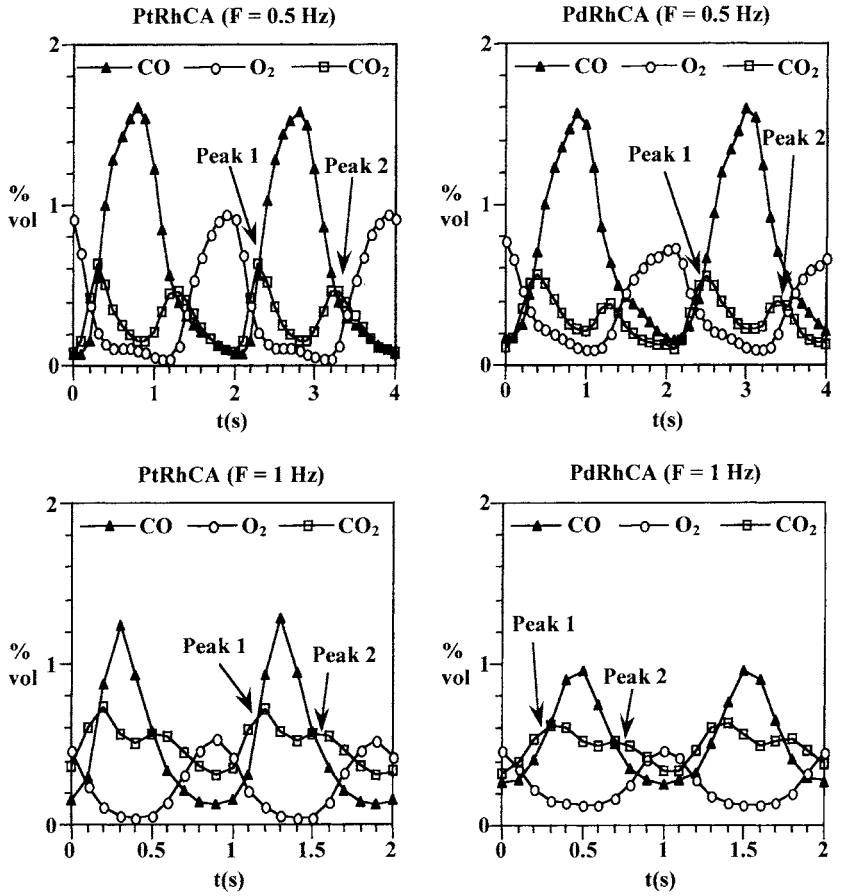

Fig. 7. Evolution of reactants (CO and O_2) and product (CO_2) upon reaction at 450°C under transient conditions ($F = 0.5$ and 1 Hz) on bimetallic PtRh/CeO_2-Al_2O_3 (PtRhCA) and PdRh/CeO_2-Al_2O_3 (PdRhCA) catalysts.

conditions. Alternate 2% CO or 1% O_2 pulses are injected on the catalyst at a frequency of 1 or 0.5 Hz for 10 min (step (i), see Fig. 1). To understand what follows, one must keep in mind that, at every gas change, both gases (CO and O_2) coexist in the gas phase for a fraction of a second. In those conditions, CO catalytic oxidation with gaseous oxygen may occur ($CO_{2\,ox}$). Looking at CO_2 formation, one will have to make the difference between CO_2 originating from the CO catalytic oxidation using gaseous oxygen ($CO_{2\,ox}$) and CO_2 coming from the reverse oxygen storage reaction ($CO_{2\,OSC}$).

In all cases, CO_2 formation occurs after every gas change. One CO_2 formation peak ($CO_2(1)$) appears going from O_2 to CO (peak 1, see Fig. 7). In this case the catalyst is partially oxidized before the introduction of CO. This CO_2 formation peak includes CO_2 coming from both the catalytic oxidation of CO in the presence of gaseous oxygen ($CO_{2\,ox(1)}$) and the oxygen storage reverse reaction ($CO_2(1) = CO_{2\,ox(1)} + CO_{2\,OSC}$). The second CO_2 formation peak ($CO_2(2)$) forms when CO is replaced by O_2 in the gas feed (peak 2, see Fig. 7). In that case, the catalyst is partially reduced. Here, the only reaction responsible for the formation of CO_2 is the catalytic oxidation of CO ($CO_2(2) = CO_{2\,ox(2)}$): upon step change from 0 to 1% O_2 (step (v), see Fig. 1) practically no CO_2 evolution was observed. These observations indicate that CO oxidation kinetics are governed by the catalyst state: oxidized or reduced. In fact, CO_2 formation related to the oxygen storage process ($CO_{2\,OSC}$) only occurs on the oxidized catalyst when O_2 is replaced by CO (peak 1). In the course of a switch from CO to O_2, oxygen storage occurs: an oxygen uptake is observed but no CO_2 forms. Furthermore, we may see from Tables 4–7 that $CO_{2\,ox(1)} \neq CO_{2\,ox(2)}$.

Examples are given in Fig. 7 for PtRh/CeO_2-Al_2O_3 (PtRhCA) and PdRh/CeO_2-Al_2O_3 (PdRhCA). The evolution of the gas phase composition (CO, O_2 and CO_2) at the reactor outlet is presented as a function of time. One can see that an increase of the alternating frequency does not modify the qualitative results. The resolution between peak 1 ($CO_2(1)$) and peak 2 ($CO_2(2)$) is just harder in some cases, when the reactivity of the catalyst is high. For comparison, the evolution of CO_2 formation as a function of time is presented in Fig. 8 for Pd-based catalysts (series 2) and in Fig. 9 for Pt-based catalysts (series 1).

Quantitative information may be obtained from the integration of the CO, O_2 and CO_2 profiles. In the case of CO_2 formation, the so-called peaks 1 and 2 were integrated separately. To calculate the total amount of CO_2 produced from the CO catalytic oxidation ($CO_{2\,catalytic}$), the amount of CO_2 originating from the reverse oxygen storage reaction must be subtracted from peak 1 ($CO_2(1)$). For that purpose, OSC values (OSC_{step}) were estimated from the data acquired in the course of step (iii) (see Fig. 1) in the second part of the experiment (CO step). To compare values after the same contact time, OSC_{step} was taken to be

Table 4
Determination of the different contributions to the CO_2 formation ($CO_2(1)$, $CO_2(2)$ and $CO_{2\,catalytic}$) from the total amount CO and O_2 consumed (CO and O_2) and the total amount of CO_2 formed (CO_2) during one period of time (1 s) under transient conditions at 450°C for series 1 samples[a]

Catalyst	CO[b]	O_2[b]	CO_2[b]	OSC_{step}[c]	$CO_2(1)$[d]	$CO_2(2)$[e]	$CO_{2\,catalytic}$[f]
PtA	16.5	15.8	15.3	0.1	7.5	7.9	15.3
RhA	17.2	16.6	16.7	0.3	8.6	8.1	16.4
PtRhA	19.1	18	17.4	0.3	8.4	9.0	17.1
PtCA	16.8	15.8	15.4	0.3	7.3	8.1	15.1
PtRhCA	17.8	17.6	16.7	2.4	9.2	7.6	14.4
RhCA	24.8	24.8	23.9	3.5	−[g]	−[g]	20.4

[a] Bimetallic PtRh-based alumina (A) and ceria-alumina (CA) supported catalysts.
[b] Expressed either in μmol CO g^{-1} or in μmol O g^{-1} or in μmol CO_2 g^{-1}.
[c] Determined from stationary regime measurements: $OSC_{step} = Q_{0.5}$ (see Table 3).
[d] Determined from the integration of peak 1.
[e] Determined from the integration of peak 2.
[f] $CO_{2\,catalytic} = (CO_2(1) - OSC_{step}) + CO_2(2)$.
[g] Peaks could not be differentiated.

Table 5
Determination of the different contributions to the CO_2 formation ($CO_2(1)$, $CO_2(2)$ and $CO_{2\,catalytic}$) from the total amount of CO and O_2 consumed (CO and O_2) and the total amount of CO_2 formed (CO_2) during one period of time (2 s) under transient conditions at 450°C for series 1 samples[a]

Catalyst	CO[b]	O_2[b]	CO_2[b]	OSC_{step}[c]	$CO_2(1)$[d]	$CO_2(2)$[e]	$CO_{2\,catalytic}$[f]
PtA	16.1	16.4	15.6	0.2	6.6	9.1	15.5
RhA	19.3	18.8	18.3	0.6	9.7	8.5	17.6
PtRhA	19.1	24.2	19.1	0.6	8.4	10.7	18.5
PtCA	19.6	20.0	19.0	0.7	8.3	10.7	18.3
PtRhCA	20.0	19.8	19.4	5.2	9.8	9.5	14.1
RhCA	25.9	26.2	25.3	7.9	13.6	11.7	17.4

[a] Bimetallic PtRh-based alumina (A) and ceria-alumina (CA) supported catalysts.
[b] Expressed either in μmol CO g^{-1} or in μmol O g^{-1} or in μmol CO_2 g^{-1}.
[c] Determined from stationary regime measurements: $OSC_{step} = Q_1$ (see Table 3).
[d] Determined from the integration of peak 1.
[e] Determined from the integration of peak 2.
[f] $CO_{2\,catalytic} = (CO_2(1) - OSC_{step}) + CO_2(2)$.

Table 6
Determination of the different contributions to the CO_2 formation ($CO_2(1)$, $CO_2(2)$ and $CO_{2\,catalytic}$) from the total amount CO and O_2 consumed (CO and O_2) and the total amount of CO_2 formed (CO_2) during one period of time (1 s) under transient conditions at 450°C for series 2 samples[a]

Catalyst	CO[b]	O_2[b]	CO_2[b]	OSC_{step}[c]	$CO_2(1)$[d]	$CO_2(2)$[e]	$CO_{2\,catalytic}$[f]
PdA	14.0	14.2	13.7	0.2	7.3	6.4	13.5
PdCA	14.4	13.9	13.7	0.8	7.4	6.3	12.9
PdRhA	14.7	14.2	14.0	0.2	8.4	5.6	13.8
PdRhCA	16.6	17.0	16.6	1.1	9.6	7.0	15.5

[a] Bimetallic PdRh-based alumina (A) and ceria-alumina (CA) supported catalysts.
[b] Expressed either in μmol CO g^{-1} or in μmol O g^{-1} or in μmol CO_2 g^{-1}.
[c] Determined from stationary regime measurements: $OSC_{step} = Q_{0.5}$ (see Table 3).
[d] Determined from the integration of peak 1.
[e] Determined from the integration of peak 2.
[f] $CO_{2\,catalytic} = (CO_2(1) - OSC_{step}) + CO_2(2)$.

Table 7
Determination of the different contributions to the CO_2 formation ($CO_2(1)$, $CO_2(2)$ and $CO_{2\,catalytic}$) from the total amount of CO and O_2 consumed (CO and O_2) and the total amount of CO_2 formed (CO_2) during one period of time (2 s) under transient conditions at 450°C for series 2 samples[a]

Catalyst	CO[b]	O_2[b]	CO_2[b]	OSC_{step}[c]	$CO_2(1)$[d]	$CO_2(2)$[e]	$CO_{2\,catalytic}$[f]
PdA	15.5	16.2	15.4	0.3	8.4	7.0	15.1
PdCA	18.1	18.6	17.8	1.7	10.1	7.9	16.3
PdRhA	15.6	15.6	15.4	0.4	8.9	6.6	15.1
PdRhCA	20.0	20.0	19.8	2.6	10.9	8.9	17.2

[a] Bimetallic PdRh-based alumina (A) and ceria-alumina (CA) supported catalysts.
[b] Expressed either in μmol CO g^{-1} or in μmol O g^{-1} or in μmol CO_2 g^{-1}.
[c] Determined from stationary regime measurements: $OSC_{step} = Q_1$ (see Table 3).
[d] Determined from the integration of peak 1.
[e] Determined from the integration of peak 2.
[f] $CO_{2\,catalytic} = (CO_2(1) - OSC_{step}) + CO_2(2)$.

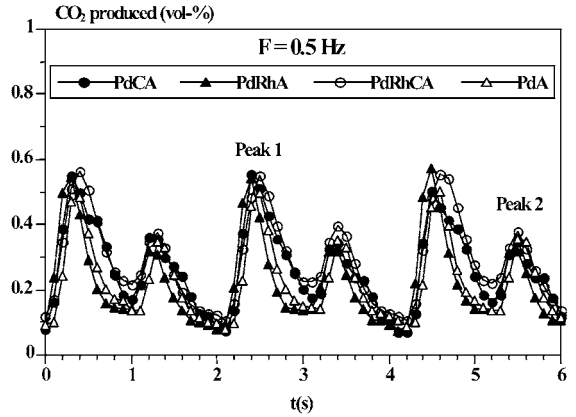

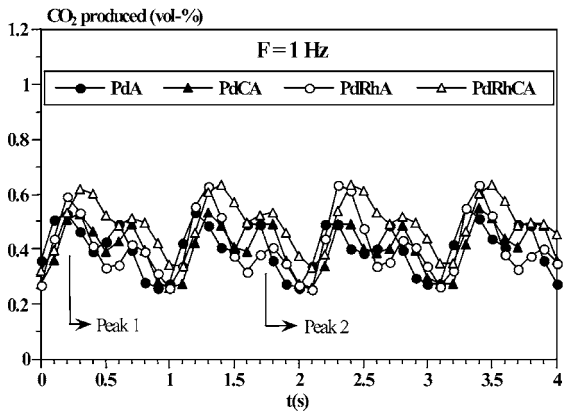

Fig. 8. Evolution of CO_2 produced under transient conditions ($F = 0.5$ and 1 Hz) upon reaction at 450°C on Pd-based alumina (A) and ceria-alumina (CA) supported catalysts.

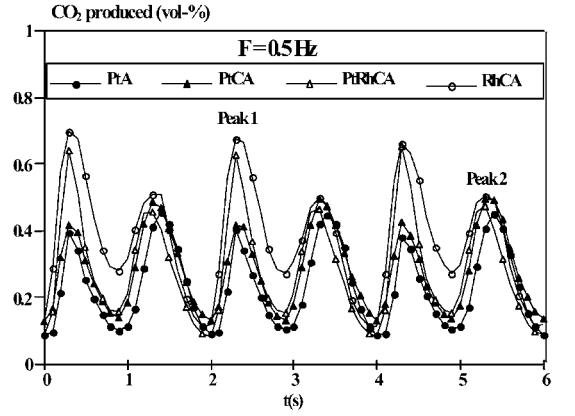

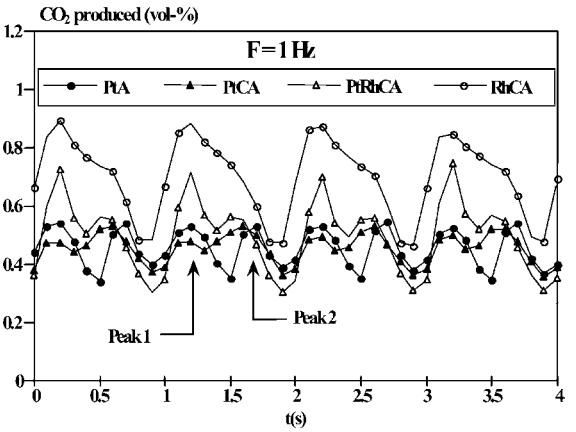

Fig. 9. Evolution of CO_2 produced under transient conditions ($F = 0.5$ and 1 Hz) upon reaction at 450°C on Pt-based alumina (A) and ceria-alumina (CA) supported catalysts.

equal to the cumulated amount of CO_2 produced after half a period of time. For example, in the case of experiments performed at 0.5 Hz, OSC_{step} is given by the integrated amount of CO_2 produced after 1 s. The average value of the calculated amounts of CO and O_2 consumed and CO_2 produced during one period of time (1 or 2 s) are displayed in Tables 4 and 5 for Pt, Rh and PtRh catalysts (series 1) and in Tables 6 and 7 for Pd-based catalysts (series 2).

From all those results we could conclude that (i) mass balance is complete and no carbon is left over the surface and (ii) oxygen storage is more sensitive to the catalyst state than the catalytic CO oxidation reaction. In fact, OSC depends on both the number and the nature of the active sites. In that case, the nature of the metal (Pt, Pd or Rh) as well as the support (alumina or ceria-alumina) are important factors. On the opposite, in the case of the $CO + O_2$ catalytic reaction, oxygen essentially comes from the gas phase. Thus, even if the catalyst has a low OSC, it will be, however, continuously fed with oxygen and the reaction may still proceed. At 450°C this reaction is fast. Moreover, the activation energy for the catalytic CO oxidation reaction was found to vary between 80 and 130 kJ mol^{-1} [24,25]. Nevertheless, the activity stays high even for strongly aged catalysts.

Looking at OSC values (OSC_{step}), catalysts may be classified in descending order as follows: Rh/CeO_2-Al_2O_3 (RhCA) > $PtRh/CeO_2$-Al_2O_3 (PtRhCA) > $PdRh/CeO_2$-Al_2O_3 (PdRhCA) > Pd/CeO_2-Al_2O_3 (PdCA) > Pt/CeO_2-Al_2O_3 (PtCA) > Rh/Al_2O_3

(RhA) $\cong$ $PtRh/Al_2O_3$ (PtRhA) > $PdRh/Al_2O_3$ (PdRhA) > Pt/Al_2O_3 (PtA) $\cong$ Pd/Al_2O_3 (PdA). Relative reactivities could be explained both by the introduction of ceria on the alumina support or by the substitution of Rh particles to Pt or Pd particles. The presence of ceria would induce a new reaction pathway through a bifunctional mechanism. CO_2 formation would derive from the reaction between an adsorbed CO molecule on the metal surface and an oxygen atom coming from the ceria surface in the vicinity of the metal particles. As a result, cerium oxide would reduce deactivation effects related to metal sintering.

Furthermore, at 450°C, Rh-based catalysts are more active than Pt- and Pd-based catalysts. The activity of the aged Rh-based catalysts would derive from both a high stability of Rh_2O_3 particles towards sintering compared to PtO_2 and PdO [8] and a better oxygen transfer from CeO_2 to Rh [7,26].

Additionally, a comparison between the amounts of CO_2 produced on Pt/Al_2O_3 (PtA) and Pt/CeO_2-Al_2O_3 (PtCA) catalysts in the course of step (i) (see Fig. 1), going from O_2 to CO (peak 1) and vice versa (peak 2), shows that $CO_2(2)$ is slightly larger than $CO_2(1)$ (Tables 4 and 5). This observation confirms that the OSC of these two catalysts must be very low. In fact, if the OSC were high, $CO_2(1)$ would be much larger than $CO_2(2)$. In these two cases, CO_2 essentially originates from the CO oxidation catalytic reaction. Moreover, considering that $CO_2(2)$ is slightly larger than $CO_2(1)$, one can conclude that CO catalytic oxidation is faster on a reduced catalyst than on a partially pre-oxidized catalyst. These two different behaviors could be related to the electronic configuration of Pt. Electronic configuration of reduced platinum may be written [Xe] f^{14} $5d^9$ $6s^1$. Both d and s orbitals are not fully occupied and electronic transfers may occur. Platinum oxide (PtO) has a [Xe] f^{14} $5d^{10}$ $6s^2$ electronic configuration. The d and s orbitals are fully occupied and electronic transfer may hardly take place. This would explain the better activity of reduced catalysts compared to oxidized catalysts.

In the case of the bimetallic PtRh-based catalysts (series 1), OSC is much higher. $CO_2(1)$ is then larger than $CO_2(2)$ and the whole amount of CO_2 produced mainly originates from the oxygen storage reverse reaction. If the contribution of the OSC to peak 1 is subtracted, peak 2 becomes larger than peak 1. This situation is the same as for Pt catalysts. For Pd catalysts, the opposite is observed. Oxidized Pd catalysts are slightly more active than the reduced ones.

This difference between $CO_2(1)$ and $CO_2(2)$ is even more pronounced when experiments are carried out at $F = 0.5$ Hz. At $F = 0.5$ Hz, CO or O_2 injections length are too short and the catalyst does not fully reduce or oxidize.

Finally, looking at the global catalytic activity of these catalysts, one can conclude that Pt catalysts are less sensitive to frequency than Pd catalysts. It is clear from Tables 6 and 7 that Pd-based catalysts (series 2) are more active in the CO catalytic oxidation when experiments are carried out at a lower frequency. This observation could indicate that Pt-based catalysts (series 1) would be more reactive, with faster response time.

4. Conclusions

Our experimental setup was shown to be appropriate for the measurement of both the OSC under transient conditions and the reactivity in the CO catalytic oxidation reaction of any catalyst. For the first time, OSC could be measured under dynamic conditions with alternate CO and O_2 pulses at frequency up to 1 Hz.

This study showed that CO_2 formation occurs after every modification in the gas phase composition. CO_2 may form on a pre-oxidized catalyst when O_2 is replaced by CO. In that case, both OSC and CO catalytic oxidation participate to CO_2 formation. Second, CO_2 is also produced on a pre-reduced catalysts when O_2 replaces CO. In that case, CO_2 exclusively originates from CO catalytic oxidation.

At 450°C, catalysts reactivity in the catalytic oxidation of CO was shown to slightly depend on the metal nature. On the opposite, OSC strongly depends on the catalysts state — oxidized or reduced. Considering the OSC value, a combination of Rh and ceria appeared to be the optimum among the catalysts under study. Relative activities were analyzed on the basis of the metal oxides relative stability and the metals electronic configuration.

Furthermore, in all cases, catalysts reduction rates under CO were shown to be smaller than the reoxidation rates under O_2. An optimized catalyst would have to have an enhance reducibility.

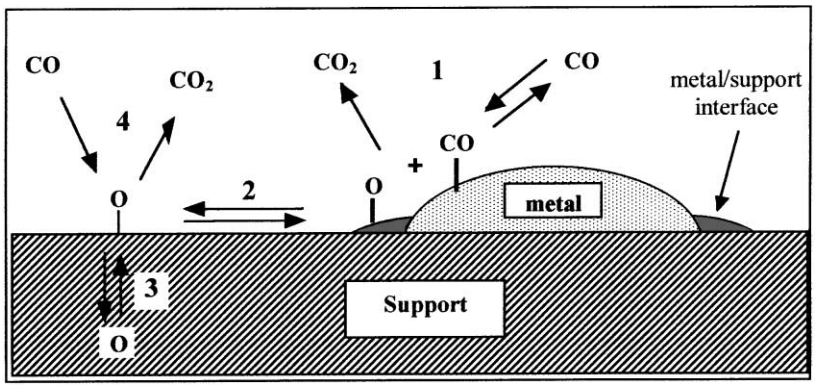

Fig. 10. Schematic representation of all processes potentially involved during OSC measurements.

Finally, based on all these observations, a general scheme of the oxygen storage process is presented in Fig. 10. CO would be activated on the metal surface and react with oxygen atoms coming from the oxide support. Oxygen transfer from the support to the metal surface would depend on both oxygen mobility at the surface (2) and in the bulk of the oxide (3) and on the metal/support interface. CO direct oxidation on the support is assumed to be very low.

References

[1] H.C. Yao, Y.F. Yu Yao, J. Catal. 86 (1984) 254.
[2] E.C. Su, C.N. Montreuil, W.G. Rothschild, Appl. Catal. 17 (1985) 75.
[3] E.C. Su, W.G. Rothschild, J. Catal. 99 (1986) 506.
[4] B. Engler, E. Koberstein, P. Schubert, Appl. Catal. 48 (1989) 71.
[5] P. Lööf, B. Kasemo, K.-E. Keck, J. Catal. 118 (1989) 339.
[6] T. Miki, T. Ogawa, M. Haneda, N. Kakuta, A. Ueno, S. Tateishi, S. Matsuuta, M. Sato, J. Phys. Chem. 94 (1990) 6464.
[7] D. Martin, R. Taha, D. Duprez, Stud. Surf. Sci. Catal. 96 (1994) 801.
[8] S. Kacimi, J. Barbier Jr., J.R. Taha, D. Duprez, Catal. Lett. 22 (1993) 343.
[9] J.-P. Cuif, G. Blanchard, O. Touret, M. Marczi, E. Quemere, SAE Technical Paper Series 961906, 1996.
[10] W.B. Clemmens, M.A. Sabourin, T. Rao, SAE Technical Paper Series 900062, 1990.
[11] J.R. Theis, SAE Technical Paper Series 961900, 1996.
[12] R. Taha, D. Duprez, N. Mouaddib-Moral, C. Gauthier, Stud. Surf. Sci. Catal. 116 (1998) 549.
[13] M. Sideris (Ed.), Methods for Monitoring and Diagnosing the Efficiency of Catalytic Converters. A Patent-oriented Survey, Studies in Surface Science and Catalysis, Vol. 115, Elsevier, Amsterdam, 1998.
[14] T. Maunula, A. Vakkilainen, A. Lievonen, K. Torkkell, K. Niskanen, M. Harkonen, SAE Technical Paper Series 993625, 1999.
[15] S. Kacimi, D. Duprez, Stud. Surf. Sci. Catal. 71 (1991) 581.
[16] R. Taha, Ph.D. thesis, Université de Poitiers, 1994.
[17] D. Martin, Ph.D. thesis, Université de Poitiers, 1994.
[18] D. Martin, R. Taha, D. Duprez, Stud. Surf. Sci. Catal. 96 (1995) 801.
[19] R. Taha, D. Duprez, Catal. Lett. 14 (1992) 51.
[20] R. Taha, D. Duprez, J. Chim. Phys. 92 (1995) 1506.
[21] E. Ruckenstein, B. Pulvermarcher, J. Catal. 38 (1977) 73.
[22] P.C. Flynn, S.E. Wanke, J. Catal. 34 (1974) 310.
[23] C.H. Bartholomew, Appl. Catal. A: Gen. 107 (1993) 1.
[24] Y.-F. Yu Yao, J. Catal. 87 (1984) 152.
[25] Y.-F. Yu Yao, Ind. Eng. Chem. Prod. Res. Dev. 19 (1980) 293.
[26] R. Taha, D. Martin, S. Kacimi, D. Duprez, Catal. Today 29 (1996) 89.